Unusual Heme Iron-Lipid Acyl Chain Coordination in *Escherichia coli* Flavohemoglobin

Paola D'Angelo,* Debora Lucarelli,* Stefano della Longa,† Maurizio Benfatto,‡ Jean Louis Hazemann,§ Alessandro Feis,¶ Giulietta Smulevich,¶ Andrea Ilari,‖ Alessandra Bonamore,‖ and Alberto Boffi‖

*Department of Chemistry University "La Sapienza", Rome, and Istituto Nazionale per la Fisica della Materia UdF, Camerino, Italy; †Department of Experimental Medicine, University of L'Aquila, L'Aquila, Italy; ‡Laboratori Nazionali di Frascati, LFN-INFN, Frascati, Italy; §Laboratoire Crystallographie CNRS, Grenoble, France; ¶Department of Chemistry, University of Florence, Sesto Fiorentino, Italy; and ‖Department of Biochemical Sciences and CNR Institute of Molecular Biology and Pathology, University "La Sapienza", Rome, Italy

ABSTRACT *Escherichia coli* flavohemoglobin is endowed with the notable property of binding specifically unsaturated and/or cyclopropanated fatty acids both as free acids or incorporated into a phospholipid molecule. Unsaturated or cyclopropanated fatty acid binding to the ferric heme results in a spectral change observed in the visible absorption, resonance Raman, extended x-ray absorption fine spectroscopy (EXAFS), and x-ray absorption near edge spectroscopy (XANES) spectra. Resonance Raman spectra, measured on the flavohemoglobin heme domain, demonstrate that the lipid (linoleic acid or total lipid extracts)-induced spectral signals correspond to a transition from a five-coordinated (typical of the ligand-free protein) to a hexacoordinated, high spin heme iron. EXAFS and XANES measurements have been carried out both on the lipid-free and on the lipid-bound protein to assign the nature of ligand in the sixth coordination position of the ferric heme iron. EXAFS data analysis is consistent with the presence of a couple of atoms in the sixth coordination position at 2.7 Å in the lipid-bound derivative (bonding interaction), whereas a contribution at 3.54 Å (nonbonding interaction) can be singled out in the lipid-free protein. This last contribution is assigned to the CD1 carbon atoms of the distal LeuE11, in full agreement with crystallographic data on the lipid-free protein at 1.6 Å resolution obtained in the present work. Thus, the contributions at 2.7 Å distance from the heme iron are assigned to a couple of carbon atoms of the lipid acyl chain, possibly corresponding to the unsaturated carbons of the linoleic acid.

INTRODUCTION

Flavohemoglobins are oxygen-binding proteins composed of a heme-containing globin domain fused with a ferredoxin reductase-like FAD- and NAD-binding module. Genes codifying for these proteins have been identified in a wide variety of bacteria and also in eukaryotic microorganisms, including yeasts and fungi (Wittenberg et al., 2002). The physiological role of flavohemoglobins is still uncertain although consensus is emerging that envisage a role in the framework of the response of the bacterial cell to oxidative or nitrosative stress (Poole et al., 1996; Gardner et al., 1998; Hausladen et al., 1998; Hausladen et al., 2001). A number of experimental observations on *Escherichia coli* flavohemoglobin (HMP) have revealed that the response to oxidative/nitrosative stress might manifest itself along different pathways that do not necessarily imply a direct NO scavenging action. Most recently, HMP has been shown to be able to bind reversibly a number of unsaturated or cyclopropanated phospholipids and fatty acids as well as liposomes obtained from *E. coli* total phospholipid extracts (Bonamore et al., 2003a). Along the same line, HMP was shown to be an efficient alkylhydroperoxide reductase, thus suggesting that the protein is involved in a specific lipid hydroperoxide repair mechanism induced by oxidative/nitrosative stress (Bonamore et al., 2003b).

The structure of the HMP-lipid complex can be inferred by comparing the three-dimensional structures of the ferrous, lipid-bound, flavohemoglobin from *Alcaligenes eutrophus* (FHP) (Ermler et al., 1995; Ollesch et al., 1999) with the ferric, lipid-free *E. coli* protein (Ilari et al., 2002). The x-ray data by Ollesch and co-workers have shown that the electron density across the distal heme pocket corresponds to a phospholipid in which the *sn-2* acyl chain is a 9,10 cyclopropane palmitoleic acid. Intriguingly, the cyclopropane ring appears to sit on the top of the iron atom at ~3.4 Å from the metal atom whereas the phosphate head of the phospholipid is hosted in a polar interdomain cavity. The x-ray structures of ferric, ligand-free, *Vitreoscilla* Hb (Tarricone et al., 1997) and HMP (Ilari et al, 2002) revealed a high degree of structural similarity with FHB and also pointed out that lipid binding contact regions are conserved in the three proteins thus suggesting that the mode of binding of the lipid is similar. Nevertheless, despite considerable efforts, crystallization of lipid-bound HMP could not be achieved under the experimental conditions in which the lipid-free derivative easily yields a number of small hexagonal crystals (Ilari et al., 2002).

To gain full understanding of the complex relationship between flavohemoglobins and phospholipids both structural investigations on the nature of protein-lipid interactions and functional studies on gene expression in response to stress stimuli need to be explored. In the present work, the fine structural aspects of HMP-lipid interaction have been

Submitted October 16, 2003, and accepted for publication January 5, 2004.

Address reprint requests to Alberto Boffi, Fax: 39-06-44-40062; E-mail: alberto.boffi@uniroma1.it.

0006-3495/04/06/3882/11 $2.00

doi: 10.1529/biophysj.103.034876

investigated by means of extended x-ray absorption fine spectroscopy (EXAFS), x-ray absorption near edge spectroscopy (XANES), resonance Raman, and ultraviolet (UV)-Vis spectroscopy. Moreover, the x-ray structure of ferric unliganded HMP has been obtained up to a resolution of 1.6 Å.

EXPERIMENTAL PROCEDURES

HMP has been expressed and purified as reported previously (Ilari et al., 2002). Protein concentration was measured spectrophotometrically using the extinction coefficient of 156,000 M^{-1} cm^{-1} at 421 nm for the ferric cyanide adduct. All reagents were from Sigma Aldrich (St. Louis, MO) with the exception of cyclopropane palmitoleic acid (Larodan Fine Chemicals, Malmö, Sweden). Lipid-free protein was prepared by passing ferric HMP on the lipid avid hydroxylalkoxypropyl-Dextran resin (Type X, Sigma Aldrich). Total *E. coli* lipid extracts (TLE) were prepared according to Bonamore et al. (2003b). Fatty acid methyl esters obtained from TLE were also analyzed by gas chromatography/mass spectrometry. According to the finding by Ollesch et al. (1999) they contained ~40% cyclopropanated fatty acids (C16:1*cyc* and C18:1*cyc*).

Cloning of the HMP heme domain

The HMP heme domain was cloned in a pET-11a-(containing the *hmp* gene) plasmid as a template for PCR amplification. Vent DNA polymerase (Fermentas) was used with the primer pairs Forward (5′-GAAGACCA-TATGCTTGACGCTC-3′) and Reverse (5′-GCGAGTAGGATCCTAAC-GACGACGACGGCTGGCGTTTTCG-3′). The 470-bp product was isolated from an agarose gel and digested with both Nde I and Bam HI. The product was then purified and ligated into the pET-11a plasmid, cut with the same restriction enzymes. The ligated product was transformed into *E. coli* BL21 (DE3) strain and the clones containing the plasmid were selected by their ability to grow in the presence of ampicillin. A recombinant plasmid screening was then performed using a control PCR and confirmed by DNA sequencing. The HMP heme domain was purified by using the first two chromatographic steps used in the whole HMP purification.

Absorption spectra were recorded on a Jasco V-570 spectrophotometer (JASCO, Tokyo, Japan). Single crystal spectra were measured with a four-dimensional x-ray system AB microspectrophotometer (Wilmot et al., 2002).

Resonance Raman measurements

Resonance Raman spectra (RR) were obtained at room temperature with excitation from the 406.7 nm line of a Kr^+ laser (Coherent Innova 302, Tampa, FL). The back-scattered light from a slowly rotating NMR tube was collected and focused into a computer-controlled double monochromator (Jobin-Yvon HG2S) equipped with a cooled photomultiplier (RCA C31034A, Lancaster, PA) and photon counting electronics. RR spectra were calibrated to an accuracy of 1 cm^{-1} for intense isolated bands with indene as the standard for the high-frequency region and with indene and CCl_4 for the low-frequency region.

EXAFS and XANES measurements and data analysis

Fe K-edge x-ray absorption spectra of lipid-free and lipid-bound HMP were collected in fluorescence mode at the BM30-B (FAME) beamline of the European Synchrotron Radiation Facility. The HMP samples were in 1:3 glycerol-water solutions buffered at pH 7 (50 mM phosphate). The final iron concentration was 4 mM and the spectra were collected at 40 K. The met-myoglobin (aquo-MetMb) solution was 7 mM (heme) in the same buffer. The storage ring was running in the two-thirds filling mode with a typical current of 170 mA. The monochromator was equipped with a Si (111) double crystal, in which the second crystal was elastically bent to a cylindrical cross section. The energy resolution at the Fe-K edge is 0.5 eV. The x-ray photon beam was vertically focused by a Ni-Pt mirror, and dynamically sagittally focused in the horizontal size. An array detector made by 24 Ge elements of very high purity was used. For each sample 10 spectra were recorded with a 7-s/point collection statistic and averaged. The spectra were calibrated by assigning the first inflection point of the Fe foil spectrum to 7111.2 eV.

The EXAFS data analysis has been performed using the GNXAS method, which is based on the theoretical calculation of the x-ray absorption fine structure signal and a subsequent refinement of the structural parameters. (GNXAS is a software package used for the x-ray absorption spectroscopy data analysis (see Filipponi et al., 1995; Filliponi and Di Cicco, 1995).)This theory allows the calculation of the interference signal in the cross section by solving the scattering of the photoelectron wave function in an effective muffin tin potential. In the GNXAS approach, the interpretation of the experimental data is based on the decomposition of the $\chi(k)$ signal into a summation over n-body distribution functions $\gamma^{(n)}$ calculated by means of the multiple-scattering (MS) theory. The theoretical framework of the GNXAS method is described in detail in previous publications (Filipponi et al., 1995; Filliponi and Di Cicco, 1995). A model cluster up to a distance cutoff of 5 Å was generated using the crystallographic coordinates of ferric HMP at 1.6 Å (see below) and of aquo-metMb (Yang and Phillips, 1996). The two-, three-, and four-body configurations in each cluster were grouped with a distance tolerance of 0.05 Å. Phase shifts were calculated using the standard muffin-tin approximation. A model EXAFS spectrum was generated by adding all the relevant single- and multiple-scattering contributions, and it was refined against the experimental data by using a least-square minimization procedure in which structural and nonstructural parameters were allowed to float. The structural parameters were the bond distance (R) and bond variance (σ_R^2) for a two-body signal, the two shorter bond distances, the intervening angle (θ), and the six covariance matrix elements for a three-body signal. The four-body configurations are described by six geometrical parameters, namely the three bond distances, two intervening angles (θ and ϕ), and the dihedral angle (ψ) defining the spatial orientation of the three bonds. Distances and angles were allowed to float within a preset range, typically ± 0.05 Å and $\pm 5°$, respectively. Two additional nonstructural parameters were minimized, namely E_0 (core ionization threshold) and S_0^2 (many body amplitude reduction factor). The quality of the fits was determined by the goodness-of-the-fit parameter R (Filipponi and Di Cicco, 1995) and by careful inspection of the EXAFS residuals and their Fourier transforms (FT). Previous investigations on model compounds have shown that a quantitative EXAFS analysis of metallo-porphyrins requires a proper treatment of MS four-body terms (Zhang et al., 1997). The inclusion of these higher order contributions is essential to obtain a good agreement between theoretical and experimental data. Moreover, the four-body MS treatment allows the extraction of additional structural information which is important in metallo-porphyrin chemistry. In particular, the quantitative determination of the structural parameters associated with the four-body distribution, provides a direct estimation of the Fe displacement from the average porphyrin plane and the distortion of the tetrapyrrole macrocycle.

A quantitative analysis of the XANES region, from 0 to 200 eV ($k \approx 7$ $Å^{-1}$) has been attempted by using the recently reported MXAN procedure (Della Longa et al., 2003; Benfatto and Della Longa, 2001) able to reproduce the experimental features of the XANES spectrum by varying selected structural parameters (MXAN is a software package used for x-ray absorption spectroscopy data analysis (see Filipponi et al., 1995; Filliponi and Di Cicco, 1995). The package works in the framework of the multiple-scattering theory (Kutzler et al., 1980; Natoli et al., 1986). To include the XANES region in the calculation and fit, the scattering matrix is calculated exactly, without any series expansion (at variance with calculations currently performed in the EXAFS region). Another important difference between the EXAFS analysis and the XANES analysis performed by the MXAN method is that the latter neglects Debye-Waller factors associated with each MS

pathway of the photoelectron. In fact, in the low energy limit (small k-values), these terms become almost temperature-independent and are equal to 1.

Inelastic scattering processes of the photoelectron produce an energy dependent damping of the spectrum that is mimicked in the MXAN procedure by a spectral convolution with a phenomenological, broadening Lorentzian function having a width $\Gamma = \Gamma_c + \Gamma(E)$. The constant part Γ_c includes the core hole lifetime and the experimental resolution, and the energy-dependent term represents all the inelastic processes. The functional form of $\Gamma(E)$ is zero below onset energy E_s, and it begins to increase from a full width of A_s. This method introduces three nonstructural parameters: Γ_c, E_s, and A_s. However, to take into account the strong asymmetry of the Fe-heme site the function $\Gamma(E)$ used to fit solution samples has a vectorial form with different values of the E_s and A_s parameters for the I_{normal} and I_{heme} components of the solution spectrum. As total, five nonstructural parameters, namely $\Gamma_c = (1.8 \pm 0.01)$ eV, $E_s^{normal} = (16.0 \pm 0.1)$ eV, $E_s^{heme} = (6.0 \pm 0.5)$ eV, $A_s^{normal} = (7.5 \pm 1.5)$ eV, $A_s^{heme} = (7.2 \pm 0.1)$ eV, are evaluated in the fitting procedure. This procedure is theoretically justified considering that all the physical quantities involved, in particular the dielectric function associated with the calculation of the self-energy of the system, must have the same symmetry of the geometrical cluster. As a consequence the mean free path term is largely anisotropic. We have verified that these nonstructural parameters are weakly correlated to the structural determination, their effect resulting just in an increase of a few percentage points of the error value reported in the tables. A constant experimental error corresponding to a noise/signal ratio of 0.01 was chosen.

Crystallization and data collection

Crystallization experiments were carried out at 25°C using the sitting drop vapor diffusion method. A volume of 2 μl of protein sample (20 mg/ml) in water was mixed with an equal amount of the reservoir solution containing 0.1 M sodium acetate buffer, pH 5.1–5.3, 21–26% polyethylene glycol 3350, and 0.2 M NaCl. Crystals grew in 1 week to $\sim 0.1 \times 0.1 \times 0.1$ mm. Data were collected as 0.5 oscillation frames on the DESY BW7B beamline in Hamburg (Germany) at a wavelength of 1.0 Å and at 100 K using 26% polyethylene glycol 200 as cryoprotectant. Data analysis performed with DENZO (Ottwinowski and Minor, 1997) indicates that the crystals are hexagonal P622 with cell dimensions of $a = b = 164.50$ Å, $c = 53.46$ Å, $\alpha = B = 90°$, and $\gamma = 120°$. The data scaling performed with SCALEPACK (Ottwinowski and Minor, 1997) gave an R_{merge} of 6.6% for 56478 unique reflections with a completeness of 98% at 1.65 Å resolution.

Structure refinement

The refinement was carried out with the maximum likelihood method incorporated in REFMAC (Murshudov et al., 1999) to an R-factor of 19.8% and an R_{free} of 24.2% at 1.65 Å resolution. The initial model used for refinement has been the low resolution x-ray structure of *E. coli* flavohemoglobin (Research Collaboratory for Structural Bioinformatics entry code 1gvh).

Water molecules and ions were added manually with the program XTALVIEW (McRee, 1993). The final model includes all 396 residues and 300 water molecules, a chlorine ion and two sodium ions. The bond lengths root mean-square deviation of 0.015 and bond angles root mean-square deviation of 2.7° have been obtained. The quality of the model was assessed using the program PROCHECK (Laskowski et al., 1993) The most favored regions of the Ramachandran plot contain 94.7% of nonglycine residues. The structural and refinement statistics are listed in Table 1.

TABLE 1 X-ray diffraction data statistics

Diffraction data	
Resolution (Å)	1.65
Unique reflections	56478
R_{merge} (%)	6.6
χ^2	1.076
Completeness (%)	98
Refinement	
R (%)	19.8
R_{free} (%)	24.2
RMS bond lengths (Å)	0.015
RMS bond angle (°)	2.7
Residues in most favored region of Ramachandran plot (%)	94.7

RESULTS

The visible absorption spectra of full-length ferric HMP and its heme domain are shown in Fig. 1 in their unliganded and linoleic acid-bound derivatives, respectively. The absorption spectra of the unliganded derivatives display a broad Soret band, characterized by a low molar absorptivity and centered at 403 nm. In the visible region, a prominent long wavelength (>600 nm) porphyrin-to-metal charge transfer band (CT 1) is observed at 645 nm both in solution and in the crystal. The solution spectra of the linoleic acid and of the TLE saturated species display a sharp peak at 407 nm and a CT 1 at 625 nm. The spectra of both derivatives were pH insensitive between pH 4.8 and 10.2. No significant temperature-dependent changes, apart from a slight band

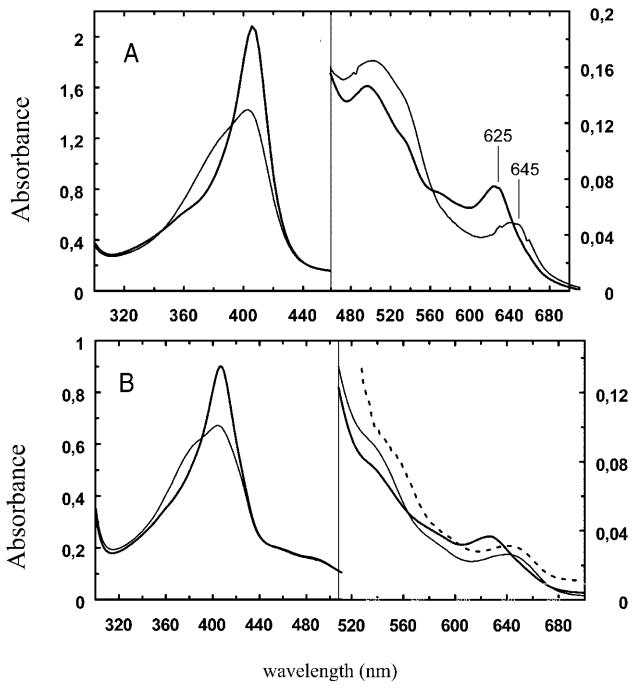

FIGURE 1 UV-visible absorption spectra of ferric *Escherichia coli* flavohemoglobin and its heme domain. The spectra of the ligand-free (*thin line*) and linoleic acid-bound (*thick line*) HMP heme domain are collected in *A*. The spectra of the ligand-free (*thin line*) and linoleic acid-bound (*thick line*) full-length HMP are collected in *B* together with the spectrum of ligand-free HMP in the crystal (*dashed line*). All spectra are in 0.1 M phosphate buffer at pH 7.0.

narrowing, were observed down to 77 K for both liganded and unliganded species (data not shown).

Resonance Raman measurements

The RR spectra reported in Fig. 2 have been obtained on the HMP heme domain. Full-length HMP could not be safely analyzed with the 406.7 nm excitation due to the strong flavin absorption at this wavelength and hence to the possible photoreduction of the flavin itself. The RR high-frequency region (Fig. 2 *B*) in which coordination and spin state marker bands are apparent in the resonance Raman spectrum is almost identical to that obtained by Mukai et al. (2001) on the full length protein. It displays the typical features of a ferric, high-spin, pentacoordinate derivative with a υ_3 band at 1492 cm^{-1}, a υ_2 peak at 1567 cm^{-1}, and υ_{10} at ~1630 cm^{-1} overlapped with vinyl stretching modes at 1623–1630 cm^{-1}. Upon linoleic acid or TLE binding (spectra *b* and *c*, respectively), the core size marker bands shift to 1478 cm^{-1} (υ_3), 1560 cm^{-1} (υ_2), and 1606 cm^{-1} (υ_{10}). In addition, a band at 1516 cm^{-1} is clearly observed (υ_{37}). These frequencies correspond to those observed for six-coordinate, high-spin, heme iron complexes. The low-frequency region (Fig. 2 *A*) displays intriguing spectral features in that lipid binding is accompanied by a strong enhancement of the 319 cm^{-1} peak with a shoulder at 305 cm^{-1}. These bands are observed at the same frequencies both with linoleic acid and with TLE phospholipids (containing mainly cyclopropanated fatty acids) thus indicating that they do not likely originate from an iron ligand stretching mode. Thus, the 319 cm^{-1} and 305 cm^{-1} bands are tentatively assigned to the γ_6 and γ_7 out-of-plane modes of the heme skeleton in analogy with myoglobin whose frequencies are observed at 337 and 305 cm^{-1}, respectively (Hu et al., 1996). However, their enhancement in the spectra of the hexacoordinate high spin heme iron is unexpected since these modes are known to be preferentially RR active in distorted hemes, such as pentacoordinate heme (Smulevich et al., 1996).

EXAFS spectra

The FT moduli of the EXAFS spectra corresponding to lipid-free HMP, (HMP_LF, *solid curve*), lipid-bound HMP (HMP_LB, *dashed curve*) and aquo-MetMb (*dotted curve*) extracted with a three-segmented cubic spline are shown in Fig. 3, lower panel. The FTs have been calculated in the interval k = 3.2–10.0 $Å^{-1}$ with no phase-shift correction applied. The high-intensity peaks R = ~1.5 Å are associated with the first coordination shell around the iron atom. In the case of lipid-free HMP it comprises four pyrrolic nitrogen atoms of the porphyrin ring (N_p) and one nitrogen atom of the proximal histidine (N_h). An additional oxygen atom contributes to this peak in the case of aquo-MetMb. The second set of peaks, between R-values of 2 and 3.5 Å contain all the single and multiple-scattering contributions associated with the carbon atoms in the second coordination shell of both the porphyrin plane and the proximal histidine. According to the crystallographic structure (see Table 1), the distal site of the heme iron in HMP is occupied by the isopropyl side chain of the LeuE11. Therefore, two additional carbon atoms of this residue contribute to the second peak of the lipid-free HMP FT spectrum at ~3.5 Å. The third set of peaks beyond 3.5 Å is mainly due to the single- and multiple-scattering contributions associated with the third shell of the tetrapyrrole macrocycle atoms.

Simple inspection of the FT spectra (uncorrected for the phase shift) offers interesting insight into the structural changes that accompany lipid binding to HMP. It can be

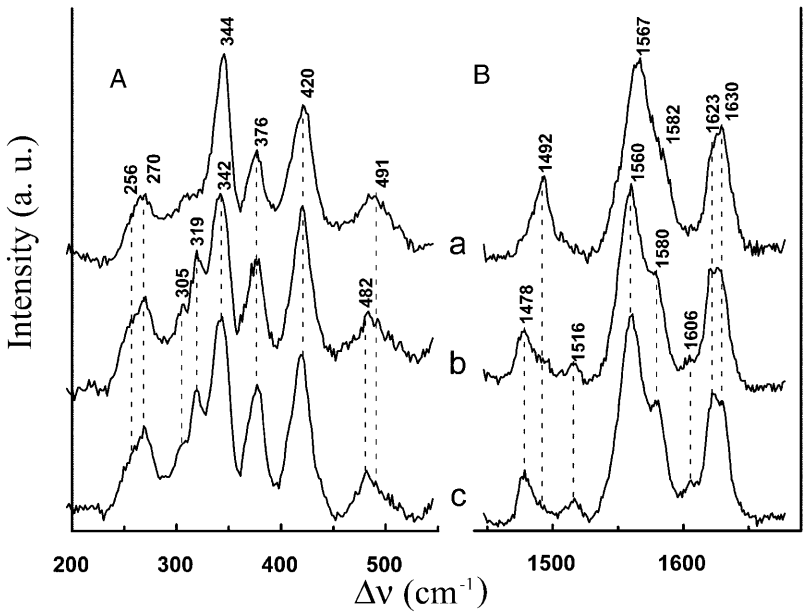

FIGURE 2 Resonance Raman spectra of ferric *Escherichia coli* flavohemoglobin heme domain. Spectra in the high frequency (*A*) and low frequency (*B*) region of lipid-free ferric HMP (*A*), linoleic acid-bound HMP (*B*) and TLE-saturated HMP (*C*). The protein concentration was 90 μM in *A* and *B* and 35 μM in *C*. Buffer was 0.1 M phosphate buffer at pH 7.0. Experimental conditions were 16-mW laser power at the sample, 5 cm^{-1} resolution. The accumulation interval ranges from 4 s/0.5 cm^{-1} to 16 s/0.5 cm^{-1}.

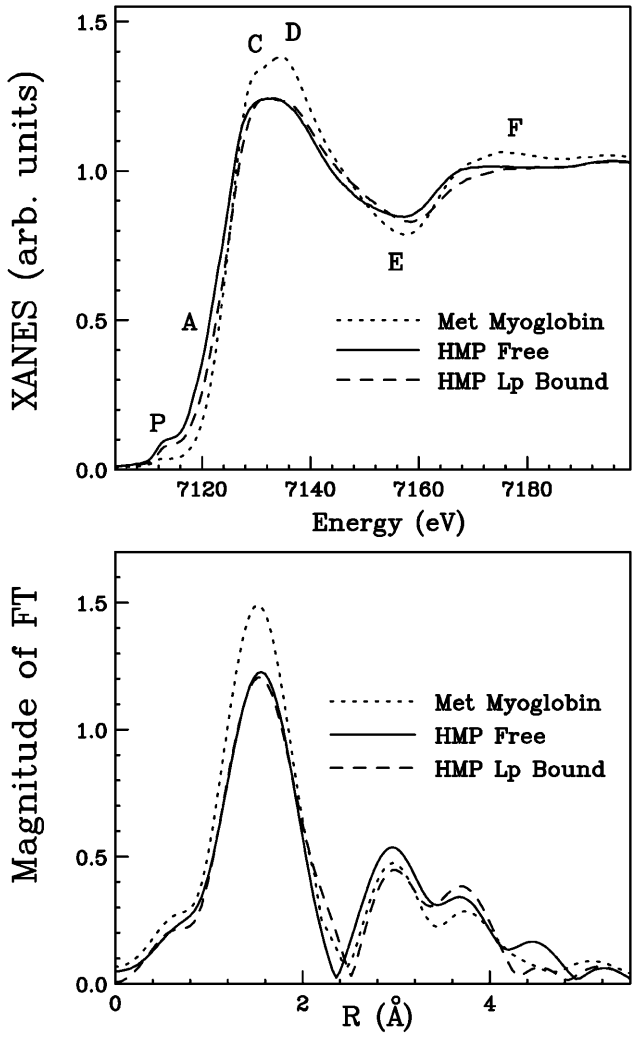

FIGURE 3 Fe K-edge XANES spectra of *Escherichia coli* flavohemoglobin. (*Upper panel*) Normalized Fe K-edge XANES spectra of lipid-free HMP (*solid line*), lipid-bound HMP (*dashed line*), and met-myoglobin (*dotted line*). (*Lower panel*) Fourier transforms of the lipid-free HMP (*solid line*), lipid-bound HMP (*dashed line*), and met-myoglobin (*dotted line*) EXAFS experimental spectra calculated in the range $k = 3.2$–10.0 Å^{-1} using a Hanning window.

noticed that both the position and intensity of the first FT peaks of liganded and unliganded HMP are identical. However, the right-hand shoulder of the first FT peak is increased and the amplitude of the second peak at $R = 3$ Å is decreased in the liganded derivative. All together these observations indicate that a structural change of the Fe environment occurs at the axial site in the presence of the lipid within an R value in the range 2.5–3.5 Å. Additional insights can be gained by looking at the FT spectrum of aquo-MetMb. In this case the contribution arising from the sixth axial ligand (right-hand shoulder at an R value within 2–2.5 Å) overlaps with the contributions of the first-shell atoms and thus greatly enhances the amplitude of the FT first peak.

A quantitative estimate of the iron coordination geometry parameters can be obtained from the analysis of the EXAFS data by means of the GNAXS program. Previous investigations on porphyrin complexes have shown that the XAS cross section can probe three-body and four-body correlation functions (Zhang et al., 1997), thus allowing a quantitative estimate of the axial shift of the metal and of the distortion of the porphyrin ring. The results of the fitting procedure applied to the lipid-free HMP EXFAS spectrum are shown in Fig. 4, left. The lipid-free HMP spectrum is dominated by the first-shell two-body signals associated with the four nitrogens from the porphyrin ($\gamma^{(2)}_{\text{Fe-Np}}$) and the axial nitrogen atom from the histidine ($\gamma^{(2)}_{\text{Fe-Nh}}$). The latter contribution was treated as a separate single-scattering (SS) signal as the Fe-N_h bond length is 0.1 Å longer than the average Fe-N_p bond length, according to the crystallographic values (see Table 1). In addition to the first-shell contributions, the simulation required four carbon atoms at ~3.4 Å derived from the connecting methylene groups ($\gamma^{(2)}_{\text{Fe}\cdots\text{Ch}}$), and two atoms at ~3.5 Å associated with the LeuE11 residue ($\gamma^{(2)}_{\text{Fe}\cdots\text{CLeu}}$, namely CD1 and CG atom of LeuE11; see also Fig. 6). The analysis of the MS terms of this system, carried out starting from the crystallographic coordinates, brings about a main contribution to the absorption coefficient arising from the MS signals of third and fourth order associated with the Fe-N_p-C_{14}-C_{23} four-body configurations. It should be pointed out that even if this scattering pathway is not linear, the amplitude of the MS signals is strongly enhanced by the porphyrin-induced multiplicity of 8. A good fit of the experimental data required the inclusion of the Fe-N_p-C_{14} three-body ($\eta^{(3)}$) and the Fe-N_p-C_{14}-C_{23} four-body ($\eta^{(4)}$) total contributions. The former term, comprising both the Fe$\cdots$$C_{14}$ SS and the Fe-Np-C_{14} three-body MS signals, is quite strong and becomes more intense at higher k. The four-body total signal $\eta^{(4)}$ has four components which are relatively equal in strength, namely the Fe$\cdots$$C_{23}$ two-body signal, the Fe-Np$\cdots$$C_{23}$ and the Fe$\cdots$$C_{14}$-$C_{23}$ three-body MS signals, and the Fe-N_p-C_{14}-C_{23} four-body MS signal. The dominant MS contribution is the Fe-Np-C_{14} three-body pathway from the porphyrin, whereas the amplitude of the MS terms associated with the histidine is negligible owing to the low multiplicity.

Fig. 4, upper left, shows the total lipid-free HMP theoretical EXAFS curve compared with the experimental data and the resulting residuals. The fitted theoretical signal closely matches the experimental data and the structural parameters obtained from GNAXS (see above) are all in agreement with the crystallographic values within the reported errors (Table 2). The accuracy of the data analysis can be also appreciated by looking at the magnitude of the FTs of the experimental, theoretical, and residual curve shown in Fig. 4, lower left.

To establish error limits on the structural parameters, we have applied a statistical analysis methodology using two-dimensional contour plots to selected parameters from the fit

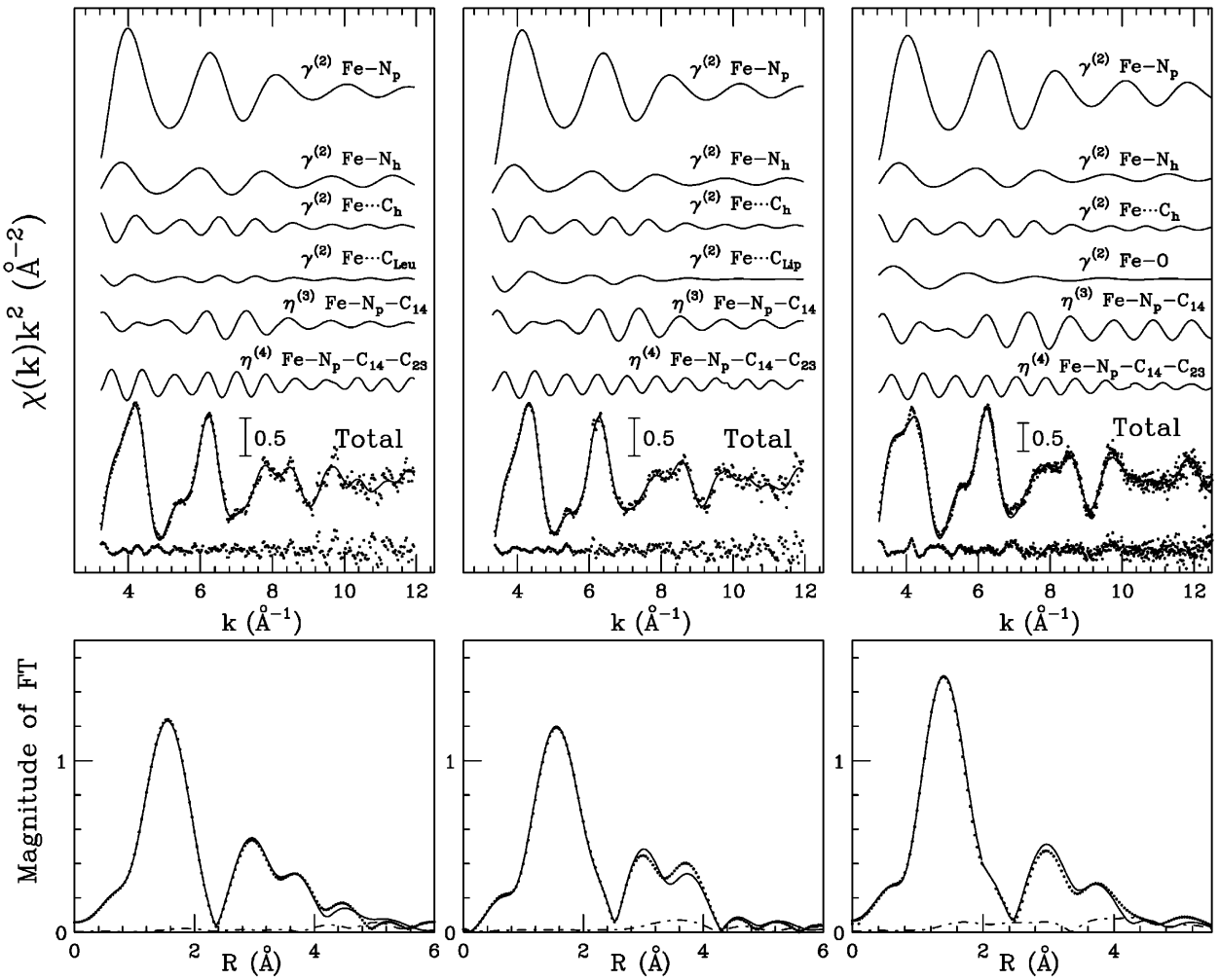

FIGURE 4 EXAFS Fourier transform spectra of *Escherichia coli* flavohemoglobin. Fit of the lipid-free HMP, lipid-bound HMP, and met-myoglobin EXAFS spectra (*left*, *middle*, and *right upper panels*, respectively). From the top to the bottom of each panel, the following curves are reported: the Fe-N_p, Fe-N_h and Fe-C_h first-shell single-scattering signals, the contributions associated with the CG and atoms of the LeuE11 residue (C_{Leu}) for lipid-free HMP, or atoms of the lipid acyl chain (C_{Lip}) for lipid-bound HMP, or a water molecule for met-myoglobin, the Fe-N_p-C_{14} total three-body signals and the Fe-Np-C_{14}-C_{23} total four-body signals. The total theoretical signals (*solid lines*) are compared with the experimental spectra (*dotted lines*) and the residual curve. The lower panels show the nonphase-shift-corrected Fourier transforms of the experimental data (*dotted line*), of the total theoretical signal (*solid line*), and of the residual curves (*dashed-dotted line*).

results. This analysis examines correlations among fitting parameters and evaluates statistical errors in the determination of the Fe coordination structure, a very useful procedure when the crystallographic data are not available. The approach is described in detail by Filipponi and Di Cicco (1995). In brief, parameters with highest correlation dominate in the error estimate. From this analysis, a strong statistical correlation between the N_p-C_{14} and C_{14}-C_{23} bond lengths has been found, suggesting that the determination of the two distances has a large effect on each other. This correlation is also observed between $R_{Fe\cdots Ch}$ and $R_{Fe\cdots CLeu}$. However, the other refined parameters were remarkably stable, varying <0.01 Å and $<1°$, for distances and angles, respectively, and giving excellent agreement with the crystallographic values. It is important to outline that the ψ-value obtained from the EXAFS analysis corresponds to a Fe displacement from the average porphyrin plane of 0.21 Å in agreement with the crystallographic value of 0.28 Å.

The analysis of the EXAFS spectrum of the lipid (linoleic acid)-bound HMP has been carried out along the line of the prior investigation, starting from the lipid-free HMP crystallographic structure. This approach is justified by the strong similarity between the FTs of the HMP experimental spectra in the absence and in the presence of the lipid, which has been previously discussed. The best-fit analysis of the lipid-bound HMP spectrum is shown in Fig. 4. Also in this case a good fit of the experimental data required the inclusion of all the SS and MS contributions associated with the porphyrin and the histidine ligand formerly described. To verify the existence of a possible interaction between the

TABLE 2 Comparison of EXAFS fit results with crystallographic values

	HMP lipid-free			HMP lipid-bound		Met-Myoglobin		
	Crystallo-graphic values (range)*	EXAFS distance/angle	EXAFS bond variance (Å^2)/angle variance (°^{2})	EXAFS distance/angle	EXAFS bond variance (Å^2)/angle variance (°^{2})	Crystallo-graphic values (range)†	EXAFS distance/angle	EXAFS bond variance (Å^2)/angle variance (°^{2})
Fe-N_p	1.96–2.04 Å	2.03(1) Å	0.008	2.02(1) Å	0.009	2.02–2.05 Å	2.03(1) Å	0.004
Fe-N_h	2.09 Å	2.11(2) Å	0.006	2.12(2) Å	0.006	2.13 Å	2.13(1) Å	0.004
Fe-O	—	—	—	—	—	2.13 Å	2.17(2) Å	0.010
Fe-C_{axial}	3.53–3.62 Å	3.50(3) Å	0.018	2.68(3) Å	0.011	—	—	—
Fe-C_h	3.43–3.48 Å	3.43(2) Å	0.010	3.41(2) Å	0.010	3.38–3.43 Å	3.43(2) Å	0.005
N-C_{14}	1.39–1.42 Å	1.42(3) Å	0.008	1.42(3) Å	0.008	1.36–1.42 Å	1.36(1) Å	0.007
C_{14}-C_{23}	1.46–1.48 Å	1.43(3) Å	0.011	1.41(4) Å	0.011	1.41–1.48 Å	1.39(4) Å	0.010
θ	126–130°	127(2)°	4	127(2)°	5	125–130°	129(2)°	4
ϕ	110–113°	111(2)°	28	113(2)°	25	107–113°	113(2)°	18
ψ	168–179°	174(2)°	4	179(2)°	4	172–178°	178(2)°	6

*Data from the 1.6 Å resolution structure obtained in the present work.
†Data from Yang and Phillips (1996).

lipid and the iron atom in the distal site, the Fe$\cdots$$C_{Lip}$ (see Fig. 6) distance was allowed to float during the minimization procedure. The best-fit geometry obtained from the EXAFS analysis foresees the presence of two atoms in the distal site at a distance of ~2.7 Å from the iron atom ($\gamma^{(2)}_{Fe}\cdots C_{Lip}$). It is important, however, to outline that owing to the similarity of the backscattering amplitudes and phases, it is not possible to distinguish among carbon, nitrogen, and oxygen atoms from the EXAFS data analysis.

Also in this case the agreement between the theoretical and experimental data is very good and the structural parameters obtained from the EXAFS analysis are close to the crystallographic values, within the reported errors (see Table 1). Interestingly, in this case a bigger value of the ψ angle has been obtained that corresponds to a Fe-porphyrin plane distance of 0.07(8) Å.

XANES spectra

The upper panel of Fig. 3 shows the XANES spectra of HMP in the absence (HMP_LF) and in the presence (HMP_LB) of the linoleic acid. The pronounced pre-edge peak (*P*) and the relative intensities of the C, D, E, and F features in the XANES spectrum of HMP_LF, are almost superimposable to those of typical high-spin pentacoordinate Fe(III)-heme compounds (Boffi et al., 1999). The XANES spectrum of the aquo-MetMb, taken as a model for high-spin hexacoordinate Fe(III)-heme compounds, is also reported. The observed differences between lipid-free HMP and aquo-MetMb are mainly focused on a blue-shift of ~2.5 eV of the rising absorption edge and have been shown to pertain to small geometrical distortions of the iron coordination sphere induced by the protein stereochemical constraints (Liu et al., 1995). The blue shift has been interpreted on the basis of different mechanisms: 1), an increase of the iron oxidation number or of its net charge, which in turn enhances the energy necessary to extract an electron from the metal (Labhardt and Yven, 1979; Sano et al., 1992; Liu et al., 1995; Yachandra, 1995); 2), the binding of a sixth ligand to a five-coordinate Fe-heme (Pin et al., 1994; Della Longa et al., 1998, 1999, 2001); and 3), a decrease of the first-shell average distance (Pin et al., 1994), and in particular of the Fe-Np bond length. Both mechanisms *2* and *3* give rise to a blue shift by changing the ligand field acting on the metal and by increasing the energy of the empty electron states with *p*-symmetry.

The lipid-induced changes of the XANES spectra are a direct proof that a bonding interaction occurs at the Fe site. The 1 eV blue-shift of the absorption rising edge (feature A) and the decrease of the *P* pre-edge peak are both in agreement with the hypothesis that lipid-bound HMP is a high-spin Fe(III)-heme compound with a weakly interacting axial ligand. In particular, as discussed in a previous work (Boffi et al., 1999), the decrease of the *P* peak, is in agreement with the experimentally observed changes from a pentacoordinate to a hexacoordinate Fe-heme system (Oyanagy et al., 1987; Shiro et al., 1990; Ikeda-Saito et al., 1992). This peak probes empty molecular orbitals with d-symmetry and becomes evident when the asymmetry of the metal coordination increases due to *p-d* mixing. In the present case, heme iron coordination results in a decrease of *p-d* mixing, and in turn a decrease of the intensity of the *P* peak.

A quantitative analysis of the XANES spectra has also been carried out as described in Materials and Methods. The same cluster (32 atoms) as in the EXAFS analysis was taken into account, and the least-square minimization was performed in the space of the three iron-ligand distances, namely the Fe-N_p distance, the Fe-N_h distance and the distance between the Fe and the sixth axial molecular group, i.e., the LeuE11 residue in lipid-free HMP, and the two

putative carbon atoms from the lipid in lipid-bound HMP. In Fig. 5, the best fitting theoretical curves (*solid line*) in the 0–200 eV energy range are shown, superimposed to the experimental data (*dashed lines*) of lipid-free HMP (HMP_LF, *upper curves*) and lipid-bound HMP (HMP_LB, *center curves*). In the lower part of the figure, the two theoretical curves are compared, to show how they reproduce the changes observed experimentally going from lipid-free HMP (*solid curve*) to lipid-bound HMP (*dashed curve*; compare with Fig. 3).

The MXAN results yielded the following parameter estimate for lipid-free HMP leading to a square residual $\chi^2_{red} = 1.46$: Fe-N_p = (2.03 ± 0.02) Å, Fe-N_h = (2.20 ± 0.07) Å, and Fe···C_{Leu} = (3.65 ± 0.12) Å. In the case of lipid-bound HMP, the following bond distances were obtained leading to a square residual $\chi^2_{red} = 1.18$: Fe-N_p = (2.04 ± 0.02) Å, Fe-N_h = (1.96 ± 0.04) Å, and Fe···C_{lip} = (2.40 ± 0.07) Å. The overall results are in good agreement with the EXAFS results, although there is a discrepancy concerning the numerical values of the axial distances of lipid-bound HMP. In particular, Fe···C_{lip} is shorter (2.4 Å) as compared to that obtained from EXAFS data analysis (2.7 Å). A possible source of systematic errors in this analysis is due to the longer mean free path of the photoelectron in the XANES energy range with respect to the EXAFS approach. Thus, other atoms, not included in the 32-atom cluster of lipid-bound HMP, might contribute to the observed XANES signal, whereas their contribution is negligible within the EXAFS limit. Second, the conformational heterogeneity of the protein lipid complex can be included in the Debye-Waller factors in the EXAFS analysis, but cannot be considered in the MXAN calculation of single cluster configurations as Debye-Waller factors are neglected in the low energy limit.

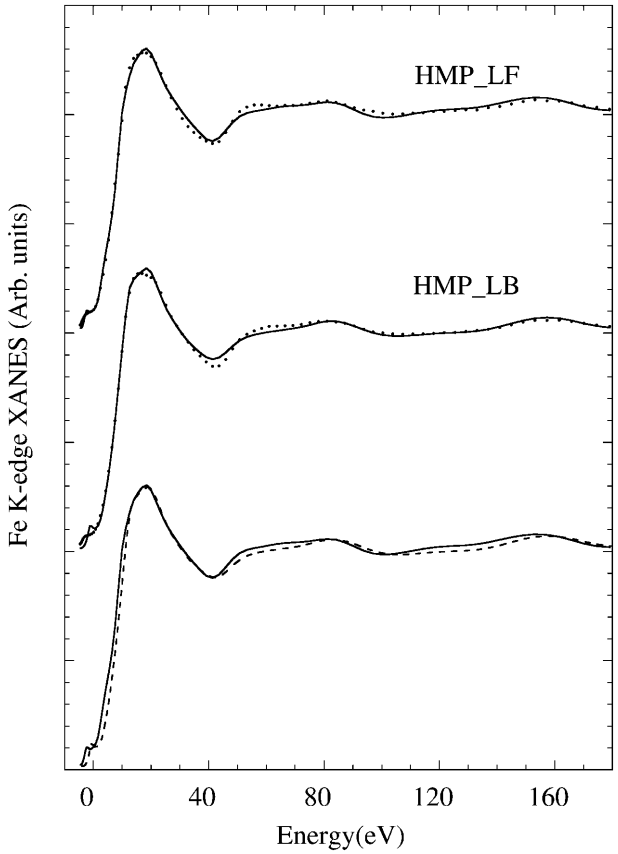

FIGURE 5 XANES spectra of *Escherichia coli* flavohemoglobin. Normalized Fe K-edge XANES spectra of lipid-free HMP (HMP_LF) and lipid-bound HMP (HMP_LB). Continuous lines refer to the best fitting theoretical curves obtained from the MXAN refinement (see Materials and Methods). Bottom spectra represent the comparison between the theoretical curves of lipid-free HMP (*solid line*) and lipid-bound HMP (*dashed line*).

DISCUSSION

The present results provide evidence for an unusual interaction between a hemoprotein ferric heme iron and the hydrocarbon acyl chain of a fatty acid. Binding of unsaturated fatty acid (UFA) or cyclopropanated fatty acid (CFA) to HMP has been previously shown to give rise to a spectral change in the visible spectrum of the ferric heme that was tentatively assigned to a transition from a five-coordinate high-spin species to a six-coordinate high-spin species (Bonamore et al., 2003b). Based on the observed spectral signals and on the structural data of Ollesch et al. (1999), it was suggested that the double bond or cyclopropane ring recognition by the flavohemoglobin involves a weak but direct bonding interaction to the heme iron atom. Nevertheless, inspection of the crystal structure of the ferrous, lipid-bound, *A. Eutropus* FHP (1.75 Å resolution) indicates that the iron-nearest carbon atom (CA of the cyclopropane ring, see Fig. 6) in ferrous, lipid-bound, FHP is at 3.5 Å distance from the metal. Such distance precludes any bonding interaction between the iron atom and the distal ligand in that no orbital overlap can be predicted to occur involving the dz^2 ferrous or ferric iron orbital at a distance higher than 3.0 Å. Interestingly, the ferric, ligand-free, HMP (1.6 Å resolution, present work) displays similar structural features within the iron first coordination shell with the CG carbon atom of LeuE11 at 3.4 Å distance from the iron atom. Thus, in ferrous lipid-bound and ferric lipid-free flavohemoglobins, the iron atom preserves a pentacoordinate stereochemistry and establishes no bonding interactions at the distal site. The present results on the ferric lipid-bound HMP complete the picture but also offer a different view. In agreement with the crystallographic data, optical absorption (both in solution and in the crystals) and resonance Raman spectroscopies point out unambiguously that the lipid-free, ferric derivative is a pentacoordinate species and the LeuE11 residue does not establish a bonding interaction with the ferric iron. In contrast, the formation of a hexacoordinate derivative is clearly demonstrated upon lipid binding to the ferric HMP protein by the low frequency shift of the core size

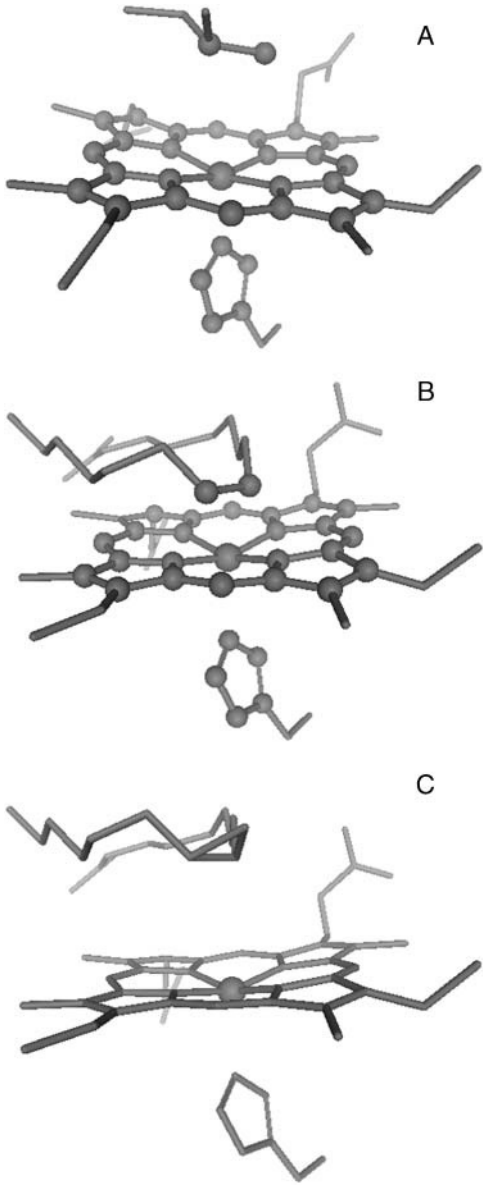

FIGURE 6 Heme iron coordination geometry in flavohemoglobins. The crystal structure of the active site of ferric, lipid-free *Escherichia coli* flavohemoglobin (*A*, PDB code:1GVH) is compared with the structure of the ferrous cyclopropane-palmitoleic-bound *Alcaligenes eutrophus* flavohemoglobin (*C*, PDB code:1CQX). The hypothetical structure of ferric, linoleic acid-bound HMP is shown in *B*. The atoms belonging to the cluster used in EXAFS and XANES data analysis are shown as spheres.

marker bands band (Choi et al., 1982; Boffi et al., 1999). The appearance of a hexacoordinate high-spin species is accompanied by an unusually intense band at 319 cm^{-1}, attributed to a γ_6 heme out-of-plane mode. The conversion from a pentacoordinate to a hexacoordinate species is consistent with the formation of an axial bonding interaction between the ferric heme iron and the lipid (linoleic acid or TLE) moiety. A previous screening (Bonamore et al., 2003a) pointed out that lipid-induced spectral changes, attributed to lipid binding, are specific for UFA and CFA free fatty acids as well as for negatively charged phospholipids esterified with a UFA or a CFA molecule. UFA or CFA methyl esters are not recognized by the protein binding site. Thus, on the basis of the structural data by Ollesch et al. (1999), an explicit model for UFA or CFA binding to HMP has been proposed in which the negatively charged part of the lipid moiety is hosted in an anion binding cavity located next to the heme pocket and the cyclopropane ring or the double bond are directly coordinated to the iron atom. To single out the nature of such an unusual iron-ligand bonding interaction XANES and EXAFS measurements have been carried out in parallel on the ligand-free and lipid-bound protein. The picture that emerges from these studies is both enlightening and intriguing. Direct inspection of the FT spectra (Fig. 3 *B*) points out that differences between the lipid-free and lipid-bound ferric protein are manifest within a shell of 2.5–3.5 Å from the iron atom. In particular, when comparing the FT spectra of ligand-free and lipid-bound HMP, an additional shoulder accompanied by an increase in intensity of the first peak can be observed in the latter spectrum. This feature is assigned to an axial contribution in the sixth coordination position in lipid-bound HMP. Quantitative analysis of the EXAFS data, carried out by means of the GNAXS program in lipid-free and lipid-bound HMP as well as in aquo-metMb provides an unequivocal structural interpretation of the spectral signal. In fact, the minimization procedure used to refine the iron-nearest neighbors distances in aquo-metMb and lipid-free HMP reproduces with high accuracy the crystallographic data available for both proteins within 4 Å from the iron core. In particular, the contribution at 2.14 Å in aquo-metMb from the iron atom is assigned to Fe-O (see Table 2; see also Yang and Phillips, 1996) and an iron-carbon distance ($Fe\cdots C_{Leu}$) of 3.4 Å in HMP. It is significant that the EXAFS profile is well accounted for very similar contributions in both aquo-metMb and lipid-free HMP, whereas it differs in the component due to the sixth coordination position ($Fe\cdots C_{Leu}$ and Fe-O, in HMP and aquo-metMb, respectively). The excellent agreement between EXAFS results and crystallographic data for aquo-metMb and lipid-free HMP strengthens the structural determination made for lipid-bound HMP and indicates that a bonding interaction does occur between the ferric heme iron and a couple of atoms located at 2.7 Å from the metal. XANES analysis, carried out on the same 32-atom cluster used in EXAFS calculations, provides a similar picture even though the axial contribution on the distal side of the iron atom appears at a shorter distance, namely 2.4 Å (see Fig. 4 and Results). The origin of the discrepancies between EXAFS and XANES calculations has been discussed in the Results section and has been attributed to the approximation used in the MXAN method. As shown in Fig. 6 and Table 1, the geometry of the atom cluster indicates that the distances obtained either by EXAFS or XANES measurements are fully compatible with the presence of

a nonvanishing overlap between the (empty) iron dz^2 orbital and a donor orbital of appropriate symmetry. The double-bond π-orbitals of the unsaturated linoleic acid chain are certainly suitable for an electron donation to the ferric iron dz^2 orbital. Nevertheless, given the highly similar spectral changes induced by the interaction of the iron atom with physiologically occurring phospholipids, mainly composed by cyclopropanated fatty acids, it should be postulated that the cyclopropane moiety is equally capable of a π-type electron donation effect. Still, the presence of an iron coordinated water molecule at 2.6–2.7 Å from the metal cannot be ruled out (Smulevich et al., 1999, and references therein). It is of interest to consider the recently reported structural analysis of the cytochrome p450 form *Bacillus subtilis* in its complex with miristic acid (Lee et al., 2003). In this protein, the carboxyl moiety of the fatty acid enters the heme pocket from a polar cavity located on the top of the distal heme side and establishes a hydrogen bonding interaction with an iron-coordinated water molecule. In the case of HMP, it might be envisaged that the distal pocket opening, induced by the lipid accommodation, allows for the entry of a water molecule. However, the highly hydrophobic nature of the distal pocket and hence the absence of a polar cavity on the top of the heme pocket in HMP, certainly does not support this hypothesis.

It is important to note that the lipid-induced spectral changes pertain uniquely to the ferric HMP derivative and the UV-Vis absorption and resonance Raman spectra of the reduced derivatives (unliganded or CO-bound) are not affected by the presence of either UFA or CFA derivatives (Bonamore et al., 2003b). Thus, the iron-lipid acyl chain interaction is a redox-dependent process in which, upon metal oxidation, a bonding interaction is established that entails a decrease in the distance between the iron and the nearest neighbor carbon atom of the lipid acyl chain from 3.5 to 2.7 Å. Although the functional counterpart of this unusual interaction is as yet unknown, we may envisage that the ferric iron-lipid acyl chain interaction plays a role within the recently identified alkylhydroperoxide reductase activity of HMP (Bonamore et al., 2003a). In this framework, the hydroperoxide moiety of the phospholipid molecule may not be recognized directly through the formation of an iron-hydroperoxide bond (it should be recalled that ferric iron in HMP is insensitive to added peroxides, including hydrogen peroxide (Ilari et al., 2002). Most likely, the substrate is first recognized by direct binding of the double bond of the lipid acyl chain to the ferric heme iron accompanied by a redox-dependent structural rearrangement. The lipid-induced structural change may thus represent the first step in the alkylhydroperoxide (in which the hydroperoxide group is located at one carbon atom distance from the double bond) reduction mechanism.

This work was supported by grants from Ministero Istruzione Università Ricerca for the Centro di Eccellenza Biologia e Medicina Molecolare and local grants to A.B. Experiments have been performed at line BM30B as part of the proposal number CH-1311.

REFERENCES

Benfatto, M., and S. Della Longa. 2001. Geometrical fitting of experimental XANES spectra by a full multiple scattering procedure. *J. Synchr. Rad.* 8:1087–1094.

Boffi, A., T. K. Das, S. Della Longa, C. Spagnuolo, and D. L. Rousseau. 1999. Pentacoordinate hemin derivatives in sodium dodecyl sulfate micelles: model systems for the assignment of the fifth ligand in ferric heme proteins. *Biophys. J.* 77:1143–1149.

Bonamore, A., A. Farina, M. Gattoni, M. E. Schininà, A. Bellelli, and A. Boffi. 2003a. Interaction with membrane lipids and heme ligand binding properties of *Escherichia coli* flavohemoglobin. *Biochemistry.* 42:5792–5801.

Bonamore, A., P. Gentili, M. E. Schininà, A. Ilari, and A. Boffi. 2003b. The flavohemoglobin from *Escherichia coli* is an efficient alkylhydroperoxide reductase. *J. Biol. Chem.* 278:22272–22277.

Choi, S., T. G. Spiro, K. C. Langry, K. M. Smith, D. L. Budd, and G. N. La Mar. 1982. Structural correlations and vinyl influences in resonance Raman spectra of protoheme complexes in proteins. *J. Am. Chem. Soc.* 104:4345–4351.

Della Longa, S., A. Arcovito, A. Congiu Castellano, M. Girasole, J. L. Hazemann, and M. Benfatto. 2003. Redox-induced structural dynamics of Fe-heme ligand in myoglobin by x-ray absorption spectroscopy. *Biophys. J.* 32:329–341

Della Longa, S., A. Arcovito, M. Girasole, J. L. Hazemann, and M. Benfatto. 2001. Quantitative analysis of x-ray absorption near edge structure data by a full multiple scattering procedure: the Fe-CO geometry in photolyzed carbonmonoxy-myoglobin single crystal. *Phys. Rev. Lett.* 87:155501/1–4.

Della Longa, S., A. Arcovito, B. Vallone, A. Congiu Castellano, R. Kahn, J. Vicat, Y. Soldo, and J. L. Hazemann. 1999. Polarised x-ray absorption spectroscopy of the low temperature photoproduct of carbonmonoxy-myoglobin. *J. Synchr. Rad.* 6:1138–1147.

Della Longa, S., S. Pin, R. Cortes, A. V. Soldatov, and B. Alpert. 1998. Fe-heme conformations in ferric myoglobin. *Biophys. J.* 75:3154–3162.

Ermler, U., R. A. Siddiqui, R. Cramm, and B. Friedrich. 1995. Crystal structure of the flavohemoglobin from *Alcaligenes eutrophus* at 1.75 Å resolution. *EMBO J.* 14:6067–6077.

Filipponi, A., and A. Di Cicco. 1995. X-ray-absorption spectroscopy and *n*-body distribution functions in condensed matter. II. Data and applications. *Phys. Rev. B.* 52:15135–15141.

Filipponi, A., A. Di Cicco, and C. R. Natoli. 1995. X-ray-absorption spectroscopy and *n*-body distribution functions in condensed matter. I. Theory. *Phys. Rev. B.* 52:15122–15130.

Gardner, P. R., A. M. Gardner, L. A. Martin, and A. L. Salzman. 1998. Nitric oxide dioxygenase: an enzymic function for flavohemoglobin. *Proc. Natl. Acad. Sci. USA.* 95:10378–10383.

Hausladen, A., A. J. Gow, and J. S. Stamler. 1998. Nitrosative stress: metabolic pathway involving the flavohemoglobin. *Proc. Natl. Acad. Sci. USA.* 95:14100–14105.

Hausladen, A., A. J. Gow, and J. S. Stamler. 2001. Flavohemoglobin denitrosylase catalyzes the reaction of a nitroxyl equivalent with molecular oxygen. *Proc. Natl. Acad. Sci. USA.* 98:10108–10112.

Hu, S., K. M. Smith, and T. G. Spiro. 1996. Assignment of protoheme resonance Raman spectrum by heme labeling in myoglobin. *J. Am. Chem. Soc.* 118:12638–12646.

Kutzler, F. W., C. R. Natoli, D. K. Misemer, S. Doniach, and K. O. Hogdson. 1980. Use of one electron theory for the interpretation of near edge structure in K-shell x-ray absorption spectra of transition metal complexes. *J. Chem. Phys.* 73:3274–3288.

Ikeda-Saito, M., H. Hori, L. A. Anderson, R. C. Prince, I. J. Pickering, G. N. George, C. R. Sanders II, R. S. Lutz, E. J. McKelvey, and R. Mattera. 1992. Coordination structure of the ferric heme iron in engineered distal histidine myoglobin mutants. *J. Biol. Chem.* 267:22843–22852.

Ilari, A., A. Bonamore, A. Farina, K. A. Johnson, and A. Boffi. 2002. The x-ray structure of ferric *Escherichia coli* flavohemoglobin reveals an unexpected geometry of the distal heme pocket. *J. Biol. Chem.* 277: 23725–23732.

Labhardt, A., and C. Yven. 1979. X-ray absorption edge fine structure spectroscopy of the active site heme of cytochrome c. *Nature*. 277: 150–151.

Laskowski, R. A., M. W. McArthur, D. S. Moss, and J. Thornton. 1993. PROCHECK: a program to check the stereochemical quality of protein structures. *J. Appl. Crystallogr.* 26:283–291.

Lee, D. S., A. Yamada, H. Sugimoto, I. Matsunaga, H. Ogura, K. Ichihara, S. Adachi, S. Y. Park, and Y. Shiro. 2003. Substrate recognition and molecular mechanism of fatty acid hydroxylation by cytochrome P^{450} from *Bacillus subtilis*. Crystallographic, spectroscopic, and mutational studies. *J. Biol. Chem.* 278:9761–9767.

Liu, H. I., M. Sono, S. Kadkhodayan, L. P. Hager, B. Hedman, K. O. Hodgson, and J. H. Dawson. 1995. X-ray absorption near edge studies of cytochrome P-450-CAM, chloroperoxidase, and myoglobin. *J. Biol. Chem.* 270:10544–10550.

McRee, D. E. 1993. Practical Protein Crystallography. Academic Press, Orlando, FL. 365–374.

Mukai, M., C. E. Mills, R. K. Poole, and S. R. Yeh. 2001. Flavohemoglobin, a globin with a peroxidase-like catalytic site. *J. Biol. Chem.* 276:7272–7277.

Murshudov, G. N., A. Lebedev, A. Vagin, K. S. Wilson, and E. J. Dodson. 1999. Efficient anisotropic refinement of macromolecular structures using FFT. *Acta Crystallogr. D*. 55:247–255.

Natoli, C. R., M. Benfatto, and S. Doniach. 1986. Use of general potentials in multiple scattering theory. *Phys. Rev. A*. 34:4682–4694.

Ollesch, G., A. Kaunzinger, D. Juchelka, M. Schubert-Zsilavec, and U. Ermler. 1999. Phospholipid bound to the flavohemoglobin from *Alcaligenes eutrophus*. *Eur. J. Biochem.* 262:396–405.

Ottwinowski, Z., and W. Minor. 1997. Processing of x-ray diffraction data collected in oscillation mode. *Meth. Enzymol.* 276:307–326

Oyanagy, H., T. Iizuka, T. Matsushita, S. Saigo, R. Makino, and Y. Ishimura. 1987. *In* X-ray Absorption Spectroscopy of Heme Iron Derivatives. A. Bianconi and D. Congiu Castellano, editors. Springer Verlag, New York. 99–106.

Pin, S., B. Alpert, A. Congiu-Castellano, S. Della Longa, and A. Bianconi. 1994. X-ray absorption spectroscopy of hemoglobin. *Methods Enzymol.* 232:266–292.

Poole, R. K., M. F. Anjum, J. Membrillo-Hernandez, S. O. Kim, M. N. Hughes, and V. Stuart. 1996. Nitric oxide, nitrite and FNR regulation of HMP (flavohemoglobin) gene expression in *Escherichia coli*. *J. Bacteriol.* 178:5487–5492.

Sano, M., S. Komorita, and H. Yamatera. 1992. XANES spectra of copper II complexes: correlation of the intensity of the 1s–3d transition. *Inorg. Chem.* 31:459–463.

Shiro, Y., F. Sato, T. Suzuki, T. Izuka, T. Matsushita, and H. Oyanagi. 1990. X-ray absorption spectral study of ferric high spin hemeproteins: XANES evidence for coordination structure of the heme iron. *J. Am. Chem. Soc.* 112:2921–2924.

Smulevich, G., A. Feis, C. Indiani, M. Becucci, and M. P. Marzocchi. 1999. Peroxidase-benzhydroxamic acid complexes: spectroscopic evidence that a Fe-H2O distance of 2.6 Å can correspond to hexa-coordinated high-spin heme. *J. Biol. Inorg. Chem.* 4:39–47.

Smulevich, G., S. Hu, K. R. Rodgers, D. B. Goodin, K. M. Smith, and T. G. Spiro. 1996. Heme-protein interactions in cytochrome c peroxidase revealed by site directed mutagenesis and resonance Raman spectra of isotopically labelled hemes. *Biospectroscopy*. 2:365–376.

Tarricone, C., A. Galizzi, A. Coda, P. Ascenzi, and M. Bolognesi. 1997. Unusual structure of the oxygen-binding site in the dimeric bacterial hemoglobin from *Vitreoscilla sp*. *Structure*. 14:497–507.

Yachandra, V. K. 1995. X-ray absorption spectroscopy and applications in structural biology. *Methods Enzymol.* 246:638–675.

Yang, F., and G. N. Phillips, Jr. 1996. Crystal structure of CO-, deoxy, and met-myoglobin at various H values. *J. Mol. Biol.* 256:762–770.

Wilmot, C. M., T. Sjogren, G. H. Carlsson, G. I. Berglund, and J. Hajdu. 2002. Defining redox state of x-ray crystal structures by single-crystal ultraviolet-visible microspectrophotometry. *Methods Enzymol.* 353: 301–318.

Wittenberg, J. B., M. Bolognesi, B. A. Wittenberg, and M. Guertin. 2002. Truncated hemoglobins: a new family of hemoglobins widely distributed in bacteria, unicellular eukaryotes and plants. *J. Biol. Chem.* 277: 871–874.

Zhang, H. H., A. Filipponi, A. Di Cicco, M. J. Scott, R. H. Holm, B. Hedman, and K. O. Hodgson. 1997. Multiple-edge XAS studies of cyanide-bridged iron-copper molecular assemblies relevant to cyanide-inhibited heme-copper oxidases using four-body multiple-scattering analysis. *J. Am. Chem. Soc.* 119:2470–2476.